Solid State Ionics 325 (2018) 228–237

Contents lists available at ScienceDirect

Solid State Ionics

journal homepage: www.elsevier.com/locate/ssi

Study of the $n = 3$ Ruddlesden-Popper phases $LnSr_3Fe_{1.5}Co_{1.5}O_{10-\delta}$ (Ln = La, Pr, Nd) as oxygen reduction electrodes by impedance spectroscopy

J. Vega-Castillo, F. Prado*

Departamento de Física, Universidad Nacional del Sur and Instituto de Física del Sur, CONICET, Av. L. N. Alem 1253, 8000 Bahía Blanca, Buenos Aires, Argentina

ARTICLE INFO

Keywords:
$LaSr_3Co_{1.5}Fe_{1.5}O_{10-\delta}$
Ruddlesden-Popper phases
Electrochemical impedance spectroscopy
Oxide mixed conductors
SOFC cathodes

ABSTRACT

The polarization resistance (Rp) of the $n = 3$ Ruddlesden-Popper phases $LnSr_3Fe_{1.5}Co_{1.5}O_{10-\delta}$ with Ln = La, Nd and Pr has been studied by Electrochemical Impedance Spectroscopy as a function of both temperature and oxygen partial pressure. The three electrodes show Rp values comparable to other Perovskite-related materials considered as candidates for cathode of solid oxide fuel cells. The lowest polarization resistance for oxygen reduction was found for $PrSr_3Fe_{1.5}Co_{1.5}O_{10-\delta}$. The impedance spectra of the three electrodes reveal the presence of two contributions which has been preliminarily identified based on the dependence of the polarization resistance of these contributions on oxygen partial pressure (pO_2) and temperature. For the intermediate frequency contribution, the rate limiting processes would be a mixture of oxygen adsorption plus charge transfer at the electrode surface with oxide ion diffusion whereas the low frequency arc would correspond to the oxygen molecule adsorption and dissociation and oxygen gas diffusion.

1. Introduction

The Ruddlesden-Popper (RP) series of phases $A_{n+1}B_nO_{3n+1}$ (A = lanthanide or alkaline earth and B = transition metal) are interlayered compounds that alternate n perovskite layers BO_3 with rock salt layers AO in their crystal structure [1]. The more usual RP phases are those with $n = 1$, 2 and 3, while the limit, $n \rightarrow \infty$, corresponds to the perovskite. In the previous years, several RP phases were proposed as cathode for Intermediate Temperature Solid Oxide Fuel Cells (IT-SOFC) because they exhibit mixed conductivity. For instance, interesting oxygen diffusion and exchange values were reported for the $n = 1$ RP phases $(La,Sr)_2NiO_{4+\delta}$ [2–4]. For these nickelates, the mechanism for oxide ion conductivity was indicated to be via interstitial oxygen atoms located at the rock salt layer [3,5]. The oxide mixed conductor properties and the performance as SOFC cathode material of the RP phases $(Ln,Sr)_{n+1}(Fe_{1-x}M_x)_nO_{3n+1}$ with $n = 2$ and 3, Ln = La, Pr, Nd, Sm, Eu, and Gd and M = Co and Ni, have also been explored [6–10]. In these materials, the incorporation of Co or Ni replacing Fe in the perovskite layers increases the electrical conductivity [6,11] and promotes the formation of oxygen vacancies at the perovskite layers, which enhances the oxide ion conductivity via a vacancy mechanism [12–14]. On the other hand, as the number n of perovskite layers in the RP crystal structure raises, the electrical and the oxide ion conductivities tend to increase as a consequence of the loss of the bi-dimensional feature of the crystal structure. Thus, from the set of RP phases that exhibit mixed conductivity those with three perovskite layers ($n = 3$) look as the most interesting to explore their electrochemical properties. For instance, Lee and Manthiram have reported that the power density obtained from a SOFC prepared with the $n = 3$ RP phase $LaSr_3Fe_{1.5}Co_{1.5}O_{10-\delta}$ as cathode electrode resulted comparable to the one obtained using the perovskite $La_{0.6}Sr_{0.4}CoO_{3-\delta}$ [8]. Kim and Manthiram [15] studied the cathode performance of the composites $NdSr_{2.5}Ca_{0.5}Fe_{1.5}Co_{1.5}O_{10-\delta}$ + GDC, and more recently Padmasree et al. [16] studied the composites of $Sr_{3.2-x}Ca_xLn_{0.8}Fe_{1.5}Co_{1.5}O_{10-\delta}$ + GDC, finding the best results for the composite with x = 0.4 and Ln = Nd.

Regarding, the kinetic of the Oxygen Reduction Reaction (ORR), Mogni et al. [17] have studied the behavior the $n = 2$ RP phases $(La,Sr)_3(Fe,Co,Ni)_2O_{7-\delta}$ phases by Electrochemical Impedance Spectroscopy (EIS). They have identified the presence of a Warburg element, which can be associated to the oxide ion diffusion in the lattice.

Aiming to expand the knowledge of the electrochemical behavior of the $n = 3$ RP phases as cathode materials we have studied the kinetic of the ORR in $LnSr_3Fe_{1.5}Co_{1.5}O_{10-\delta}$ with Ln = La, Nd and Pr by EIS on symmetrical cells. The experimental data let us to compare the features of the three compounds and to propose the limiting stages of the ORR that generate overpotentials in this kind of electrodes.

* Corresponding author.
E-mail address: fernando.prado@uns.edu.ar (F. Prado).

https://doi.org/10.1016/j.ssi.2018.08.020
Received 26 June 2018; Received in revised form 26 August 2018; Accepted 31 August 2018

2. Experimental

$LnSr_3Fe_{1.5}Co_{1.5}O_{10-\delta}$ samples with Ln = La, Nd and Pr (LSFC, NSFC and PSFC, respectively) were synthesized by a nitrate-citrate route using La_2O_3, Nd_2O_3, Pr_6O_{11}, $SrCO_3$, $Fe(NO_3)_3.9H_2O$ and $Co(NO_3)_2{\cdot}6H_2O$ as raw materials. Stoichiometric amounts of oxides and carbonate were dissolved in diluted nitric acid and then heated up until the liquid was evaporated. Fe and Co nitrates were added and the mixture was then dissolved in a solution of distilled water, citric acid and ethylene glycol. The solution was slowly heated up until a brown gel was obtained. The gel was fired at 400 °C for 2 h and the resulting powder was grinded in an agate mortar and then annealed at 1350 °C for 12 h. The purity of the as prepared powders was verified by X-ray Diffraction (XRD) in a Philips PW1700 diffractometer using CuK_α radiation and a graphite monochromator in the angular range $10 \le 2\theta \le 80^\circ$ with a counting time of 7 s per step. The crystal structures of the synthesized materials were analyzed by the Rietveld method using the FullProf software [18].

X-rays Absorption Near the Edge Spectroscopy (XANES) at the Pr L_{III}-edge was carried out in the XAFS2 beam-line facility of the Brazilian Synchrotron Light Laboratory [19]. The sample was prepared by mixing PSFC powder with boron nitride (an inert binder and weak absorbing in the energy band of the experiment) in an adequate proportion to give a total absorption ratio of about 1.5. The energy of the Pr L_{III}-edge was aligned with the K-edge of metallic Cr. The XANES data was reduced using the software Athena [20].

Commercial $Ce_{0.9}Gd_{0.1}O_{1.95}$ (GDC) powder from Praxair Specialty Ceramics was pressed into 10 mm diameter disks by pressing the powders and then sintering at 1350 °C for 3 h. After sintering, the electrolyte disks were approximately 7 mm in diameter and around 1.25 mm thick. The inks for spray deposition were prepared by mixing the corresponding ceramic powders with V006 and isopropanol in a weigh proportion of 1:1:1. Let us mention that LSFC, NSFC and PSFC raw powders heat treated at 1350 °C were ball-milled in a low speed jar mill during 24 h using zirconia balls, before preparing the inks for spraying. A very thin layer of GDC was sprayed onto both flat sides of the GDC electrolytes and then heat treated at 1300 °C. Subsequently, symmetrical cells were prepared by spraying LSFC, NSFC or PSFC ink onto the porous GDC layer of both sides of a GDC electrolyte. Cells with electrodes of different thicknesses were made for studying the influence of this variable in the electrical properties of the three compounds. All the cells were then fired at 1000 °C to adhere the electrodes.

EIS measurements were carried out in the temperature range 500 °C ≤ T ≤ 700 °C and oxygen partial pressure (pO_2) range 10^{-4} atm ≤ pO_2 ≤ 1 atm. The data acquisition was performed by an Autolab system PGSTAT 30 coupled to a module FRA2 in a frequency range of 1 MHz to 10 mHz. An AC signal of 10 mV of amplitude was applied to the cell, under zero DC polarization. Pt grids, slightly pressed on the porous electrodes were used as current collectors. For measurements as a function of the pO_2, the electrochemical cell was coupled to an electrochemical gas control system consisting of an oxygen pump and an oxygen sensor [21]. The spectra were analyzed by means of Zview software using equivalent circuits [22].

The microstructure and thickness of the porous layers were observed by Scanning Electron Microscopy (SEM) with a Zeiss LEO EVO 40XVP instrument using both secondary and backscattered electrons.

3. Results and discussion

3.1. Crystal structure

XRD data were analyzed using the Rietveld method. The crystal

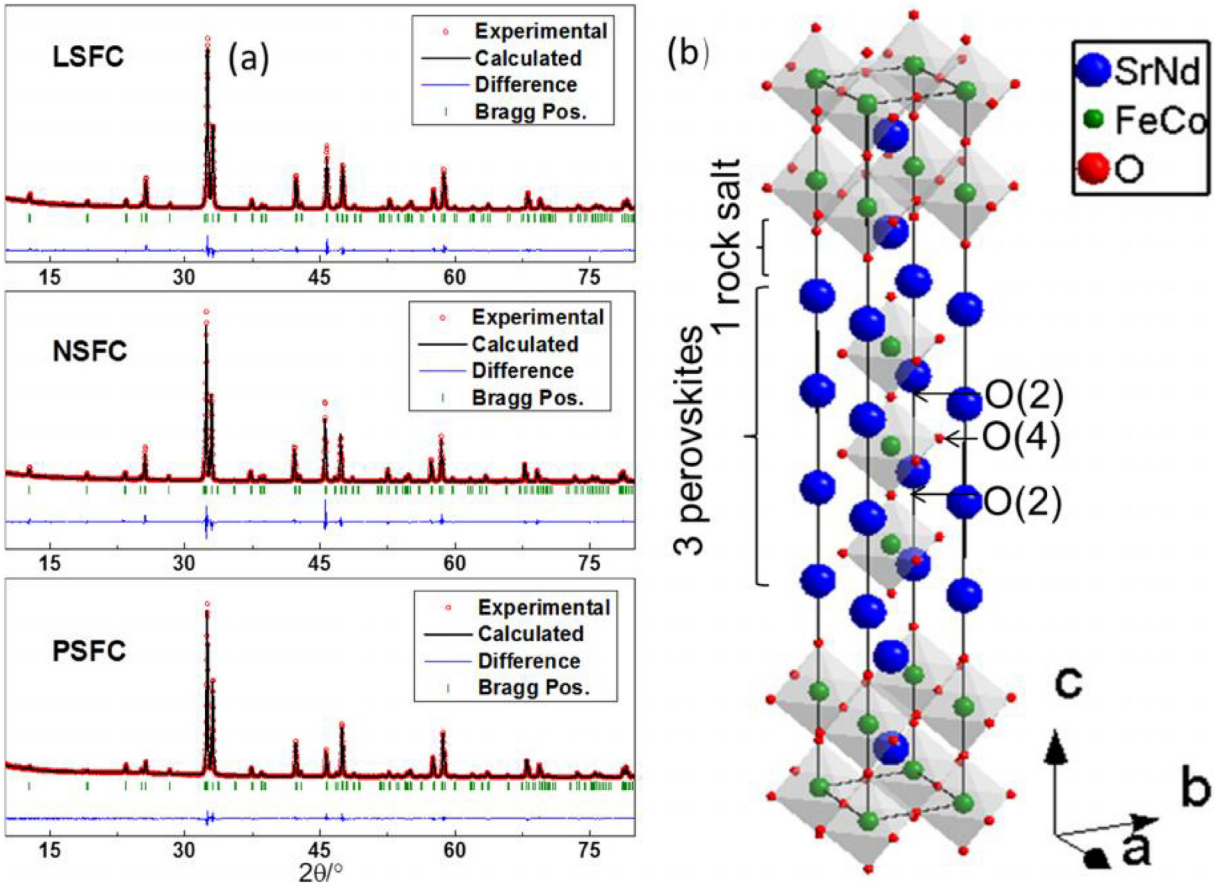

Fig. 1. (a) XRD patterns and Rietveld refinement of synthesized LSFC, NSFC and PSFC powders; (b) unit cell of LnSFC.

structures of the LSFC, NSFC and PSFC samples were refined in the tetragonal space group I4/*mmm* [13,14]. Previous analysis by Neutron Powder Diffraction (NPD) [13] and XRD [14] on LSFC show the location of oxygen vacancies at positions O(4) and O(2), which corresponds to the equatorial and apical vertices of the central (Fe|Co)O_6 octahedra, respectively. The refinement of the XRD data releasing the oxygen occupancy of these atomic positions suggested the presence of oxygen vacancies at the O(4) crystal site of the NSCF and PSCF samples. On the other hand, no evidence of oxygen vacancies at O(2) was detected for the LSCF sample in agreement with previous analysis of neutron diffraction data [13]. These results, however, represent weak evidence due to the low atomic form factor of oxygen for XRD as compared to those of La, Pr, Nd, Sr, Fe and Co. The powder XRD data, the calculated profile, and difference between them are shown in Fig. 1a. A good agreement between the experimental data and the calculated profile is observed for the three samples. No secondary phases were detected. A preferred orientation in the [001] direction is clearly observed by the enlargement of the (0 0 14) reflection at around 2θ = 45.5° for LSCF and NSCF samples. This result is not surprising given the large difference between *a* and *c* lattice parameters in the crystalline cell as shown in Fig. 1b. The values obtained for the preferred orientation parameter (Or) along [0 0 1] direction, suggest crystallites with platy habit (Or < 1) which is stronger in LSFC and NSCF.

The lattice parameters values, atomic positions, isotropic Debye-Waller factors Biso, occupancy, preferred orientation as well as reliability factors for the refinement are listed in Table 1.

The lattice parameters and the unit cell volume decrease with the replacement of La^{3+} by Pr^{3+} and Nd^{3+}. This behavior correlates with the lower ionic radius of Nd^{3+} (r_{XII} = 1.27 Å) compared to La^{3+} (r_{XII} = 1.36 Å) in coordination 12 [23]. The unit cell volume of the PSFC sample was found among those obtained for LSFC and NSFC samples. Although the ionic radius for Pr^{3+} in coordination 12 is not supplied in Ref. [23], the trend of the unit cell volume variation with the rare earth suggests the valence of Pr is 3+. In order to confirm this result, XANES spectra at the Pr L_{III}-edge for PSFC and the reference compounds $Pr(NO_3)_3$ and Pr_6O_{11} with formal Pr valence +3 and + 3.67, respectively, were recorded and are displayed in Fig. 2. The spectrum of Pr_6O_{11} shows two peaks at 5968 and 5980 eV corresponding to Pr^{3+} and Pr^{4+}, respectively [24], while the XANES signals of both $Pr(NO_3)_3$ and PSFC have only the low energy peak confirming that the valence of Pr in PSFC is 3+.

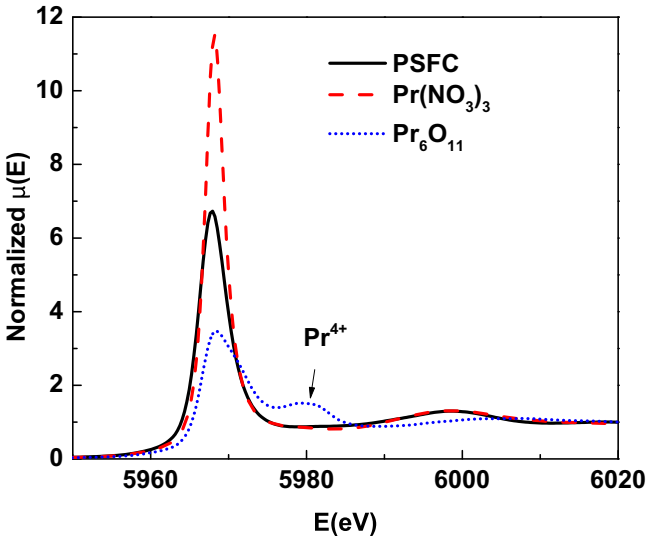

Fig. 2. XANES spectra of PSFC sample and the reference compounds $Pr(NO_3)_3$ and Pr_6O_{11} at the L_{III}-edge of Pr.

3.2. Microstructure

Fig. 3 shows SEM micrographs of the surface and cross section of the LSFC, NSFC and PSFC electrodes of the symmetrical cells used during impedance spectroscopy measurements. Fig. 3a–c show the surface of the electrodes. The thickness and uniformity of the layers forming the electrode can be observed in Fig. 3d–l. Fig. 3d, g and j show the cross sections of cells with different electrode thicknesses for LSFC electrodes. Similarly, Fig. 3e, h and k; and f, i and l show the cross section of the electrodes for NSCF and PSCF, respectively. For the three compositions the thicknesses of the electrodes vary from < 10 μm to approximately 20 μm. No delamination was detected during impedance measurements.

Table 1
Crystallographic parameters and reliability factors from Rietveld refinements of LSFC, NSFC and PSFC in space group I4/mmm[a].

			$La_3SrFe_{1.5}Co_{1.5}O_{10-\delta}$	$Pr_3SrFe_{1.5}Co_{1.5}O_{10-\delta}$	$Nd_3SrFe_{1.5}Co_{1.5}O_{10-\delta}$
a/Å			3.8416(1)	3.8294(1)	3.8257(1)
c/Å			27.862(1)	27.7834(1)	27.752(1)
V/Å^3			411.185	407.42	406.188
Ln/Sr (1)	4e	z	0.5683(1)	0.5685 (1)	0.5686 (1)
		B/Å^2	1.15 (5)	1.01 (3)	1.45 (4)
Ln/Sr (2)	4e	z	0.7011(1)	0.7012 (1)	0.7011 (1)
		B/Å^2	0.71 (5)	0.57 (4)	1.02 (4)
Fe/Co (1)	2a	B/Å^2	1.0 (1)	0.59 (8)	1.1 (1)
Fe/Co (2)	4e	z	0.1388 (1)	0.1393 (1)	0.1393 (1)
		B/Å^2	0.91 (8)	0.82 (6)	1.13 (7)
O (1)	8 g	z	0.1387 (2)	0.1392 (2)	0.1399 (2)
		B/Å^2	1.6 (2)	1.2 (2)	1.5 (2)
O (2)	4e	z	0.0693 (4)	0.0687 (3)	0.0692 (3)
		B/Å^2	1.5 (5)	1.1 (2)	1.7 (2)
O (3)	4e	z	0.2098 (3)	0.2106 (3)	0.2089 (3)
		B/Å^2	0.9 (3)	1.4 (2)	2.4 (3)
O (4)	4c	B/Å^2	1.7(5)	1.0 (3)	2.4 (3)
		Occ	1	0.94	0.86
Or [0 0 1]			0.49	0.86	0.56
Rp/%			13.1	9.89	10.3
Rwp/%			13.8	8.78	10.8
Re/%			2.19	2.68	2.24
χ^2			3.96	1.06	2.24

[a] Atomic positions are (Ln/Sr)(1) (0,0,1/2), La/Sr (2) (0,0,z), Fe/Co (1) (0,0,0); Fe/Co (2) (0,0,z), O(1) (0,1/2,z), O(2) (0,0,z), O(3) (0,0,z) and O(4) (0, 1/2,0).

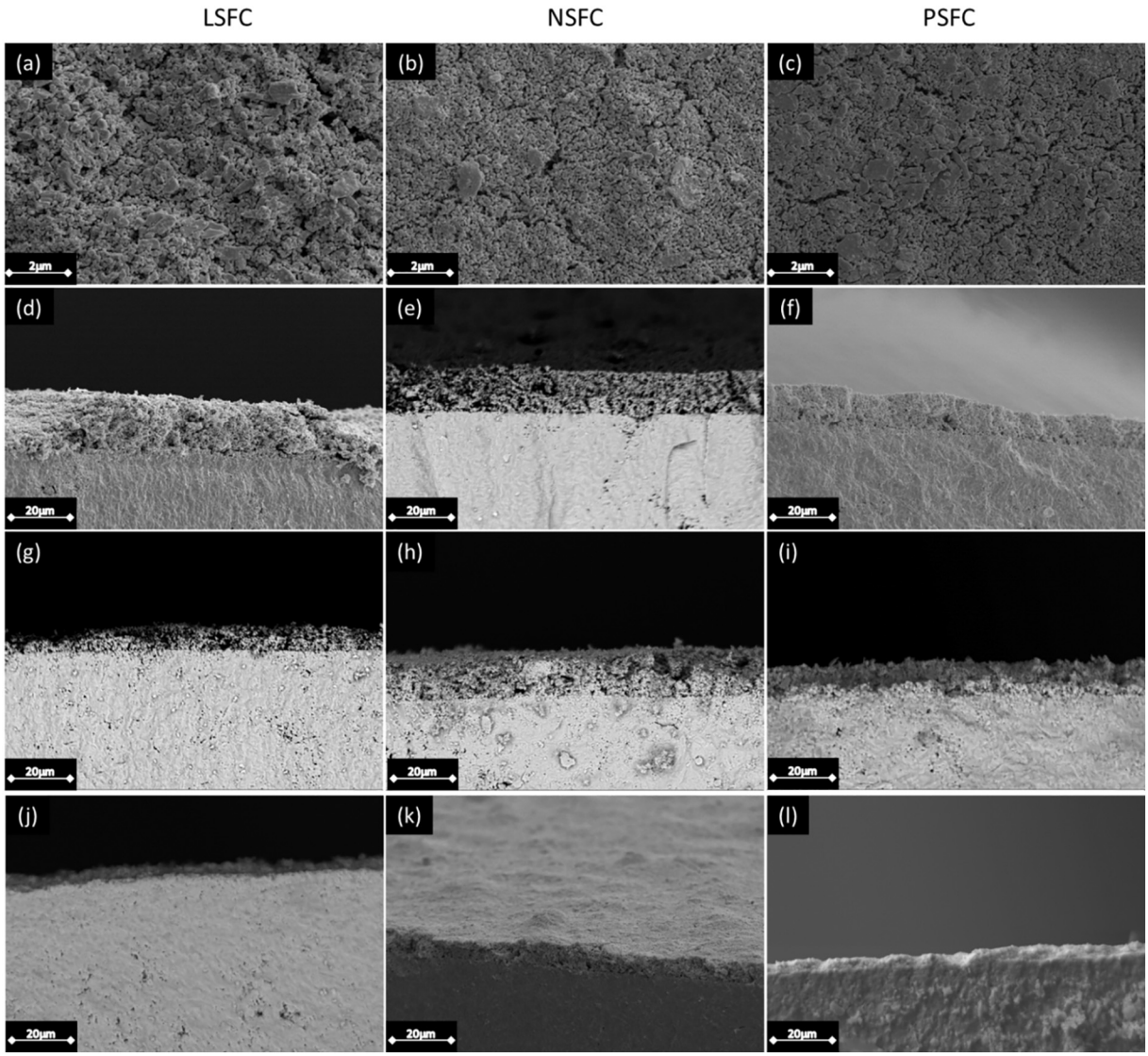

Fig. 3. SEM images of three symmetrical cells used for EIS studies with LSFC, NSFC and PSFC as electrodes from: top view (a), (b) and (c); lateral view of cross section of cells with different electrode thicknesses (d)–(f).

3.3. Electrochemical analysis

Fig. 4 displays the variation with temperature of the total polarization resistance (Rp) of symmetrical cells prepared with LSFC, NSFC and PSFC electrodes. In order to determine the effect of the electrode layer thickness in the electrochemical performance of these materials, three cells varying the electrode thickness between 5-9 μm and 17-20 μm were studied and the obtained data is shown in Fig. 4. The measurements were carried out in flowing synthetic air.

The total Rp was obtained by fitting the impedance spectra using an equivalent circuit whose characteristics are discussed in detail forward in this section. Fig. 4a shows Rp values obtained for the LSFC electrodes. A decrease of Rp is observed as the thickness of the electrode layer increases from 5 μm to 20 μm, suggesting the characteristic depth of the electrode $l_\delta \geq 20$ μm [25,26]. However, for the two other compounds, the variation of the electrode thickness does not play such a significant role, at least in the studied range of temperature. For instance, the Rp values obtained for NSCF and PSCF electrodes with thicknesses in the range 9–19 μm and 6–17 μm, respectively, yield Rp values with little variation as shown in Fig. 4b and c. In both cases, the Rp values are comparable to those observed for the 20 μm thick LSFC electrode. This behavior suggests that for NSFC and PSFC the characteristic depths are shorter than that of the LSCF material. Regarding the $n = 3$ RP phases, Padmasree et al. [16] have reported the total polarization resistance of cathode electrodes prepared with $Sr_{3.2-x}Ca_xLn_{0.8}Fe_{1.5}Co_{1.5}O_{10-\delta}$ (x = 0 and 0.4 and Ln = La, Nd, Pr) and GDC, deposited on GDC as electrolyte. They have obtained the lowest polarization resistance for the material with x = 0.4 and Ln = Nd. In Fig. 5 we compare the Rp values obtained for LSFC, NSFC and PSFC electrodes ~20 μm thick with the experimental data reported for $Sr_{3.2-x}Ca_xNd_{0.8}Fe_{1.5}Co_{1.5}O_{10-\delta}$ (x = 0 and 0.4) in composite with GDC [16]. Differences between the Rp values of both set of samples should be related to variations in the materials synthesis route, ink preparation, electrode design and deposition method that lead to different microstructures, however our experimental data indicate the lowest Rp values in this range of temperature correspond to the PSCF electrode. Hereafter, further analysis of the electrochemical performance of LSFC, NSFC and PSFC electrodes correspond to experimental data obtained for cells prepared with the thickest ones (~20 μm), whose cross sections are displayed in Fig. 3d–f.

Fig. 6 shows the variation of the impedance spectra with the oxygen partial pressure 6×10^{-4} atm $\leq pO_2 \leq 1$ atm at various temperatures between 500 and 700 °C for a symmetrical cell prepared with NSFC electrodes. See Figs. S1 and S2 for the impedance spectra obtained for

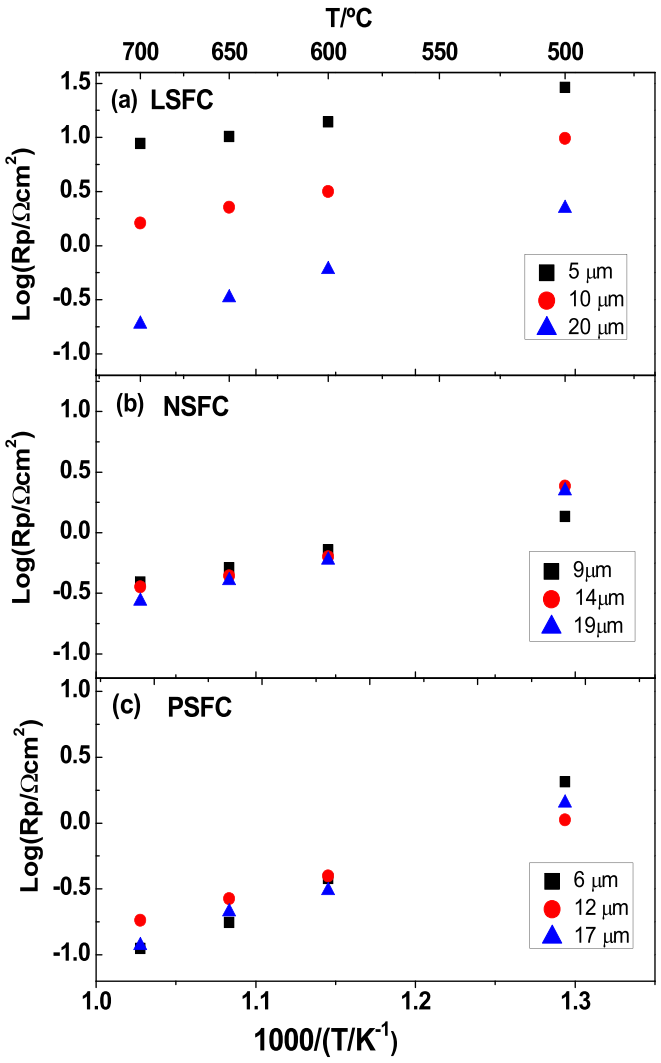

Fig. 4. Arrhenius plots of the total ASR measured in air for symmetrical cells of (a) LSFC, (b) NSFC and (c) PSFC as electrodes with different thicknesses.

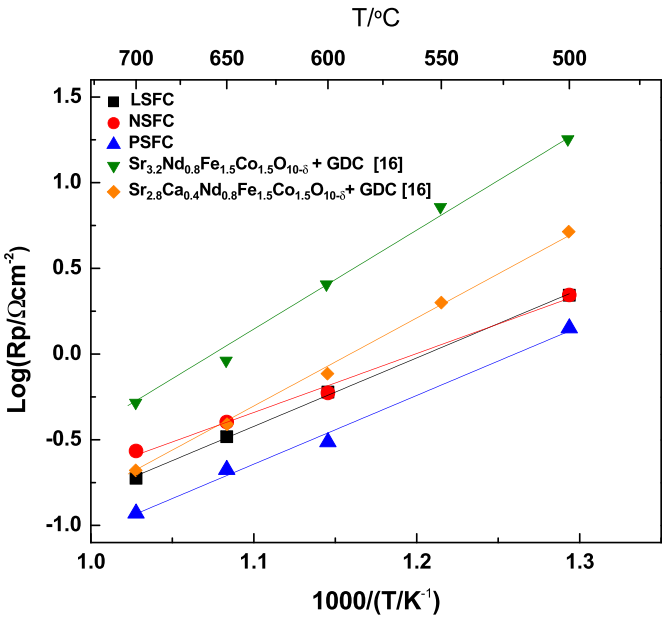

Fig. 5. Arrhenius plots of the total ASR of LSFC, NSFC and PSFC symmetrical cells with 20 μm of electrode thickness, compared to those reported for electrode composites of $Sr_{3.2-x}Ca_xLn_{0.8}Fe_{1.5}Co_{1.5}O_{10-\delta}$ (x = 0 and 0.4, Ln = La, Nd and Pr) and GDC [16].

symmetrical cells prepared with LSCF and PSCF, respectively. Indistinctly of the cell temperature, the impedance spectra under pure oxygen $pO_2 = 1$ atm consist of only one arc, while at lower pO_2 a second arc shows up in the low frequency range, that means at the right side of the shown Nyquist plots in Fig. 6. As pO_2 decreases, the diameters of both arcs increase, although the low frequency arc increases faster. The impedance data were reproduced using an equivalent circuit composed by an inductance L in series with the ohmic contribution R of the electrolyte and in series with elements representing the impedance arcs observed at low and intermediate frequency. No impedance arc at high frequency was detected. For the low frequency (LF) contribution we used a resistor in parallel with a Constant Phase Element (R||CPE), while for the intermediate frequency contribution (IF) we tried different types of circuits: another (R||CPE), a Warburg element (W) and a Gerischer element. The Warburg element is associated to diffusive processes and was used to fit one of the contributions to the impedance spectra measured in electrodes prepared with the $n = 2$ RP phases $Sr_3FeMO_{6+\delta}$ (M = Fe, Co, Ni) [17], while the Gerischer element was proposed to describe the co-limitation of bulk oxide ion diffusion and surface reaction at the surface cathode [25]. The fit obtained with the Gerischer element was poor in comparison to that obtained with either a (R||CPE) or Warburg element (W). Fig. 7a and b show, as example, the fits of the impedance spectra obtained at $T = 600\,^{\circ}C$ and $pO_2 = 6 \times 10^{-4}$ atm for the NSFC cell when the equivalent circuit includes a W_{IF} or a $R||CPE_{IF}$ element, respectively. It can be seen that the quality of the fit show little or no differences (χ^2 values are very close).

Upon fitting all the measured impedance spectra, the variation of the polarization resistance with pO_2 for each contribution was analyzed using the power law,

$$R = K \times (pO_2)^m \tag{1}$$

where K is a constant and the parameter m is related with the species involved in the electrode reaction and the process responsible of the electrode polarization [27–30]. In the case of the intermediate frequency contribution, the dependence of Rp on pO_2 yielded an exponent value m in the range $-0.35 \leq m \leq -0.2$, regardless the circuit element used, R||CPE or W. However, the impedance of the R||CPE elements calculated using the relation,

$$Z_{CPE}(\omega) = \frac{1}{B(j\omega)^p} \tag{2}$$

where B is a constant independent of the frequency and p an exponent that can have values between $p = 1$ for a pure capacitor and $p = 0$ for a simple resistor, yielded p values varying from 0.6 to ~0.5 as pO_2 decreases, which corresponds to a depleted impedance arc that shifts the apex frequency to misleading low values. This behavior suggests the intermediate frequency contribution should be associated to a non-uniform diffusion process [31]. Nonetheless, the experimental data shows that R_{IF} increases as the pO_2 decreases, which means the ionic conductivity decays as the oxygen vacancy concentration increases. The equation that describes the ionic conductivity for a non-stoichiometric oxide is [32]:

$$\sigma_{ion} = \frac{A}{T} c(1-c) \exp\left(-\frac{\Delta H_m}{k_B T}\right) \tag{3}$$

where A includes constants, geometric factors and terms independent of temperature, ΔHm is the migration enthalpy and c is the fraction of unoccupied oxygen crystal sites. It can be seen that σ_{ion} follows a negative quadratic with c. Thus, at constant temperature, if c is < 0.5, σ_{ion} should increase as the oxygen vacancy concentration increases. NPD [13] has shown the oxygen ion diffusion in these materials is via a

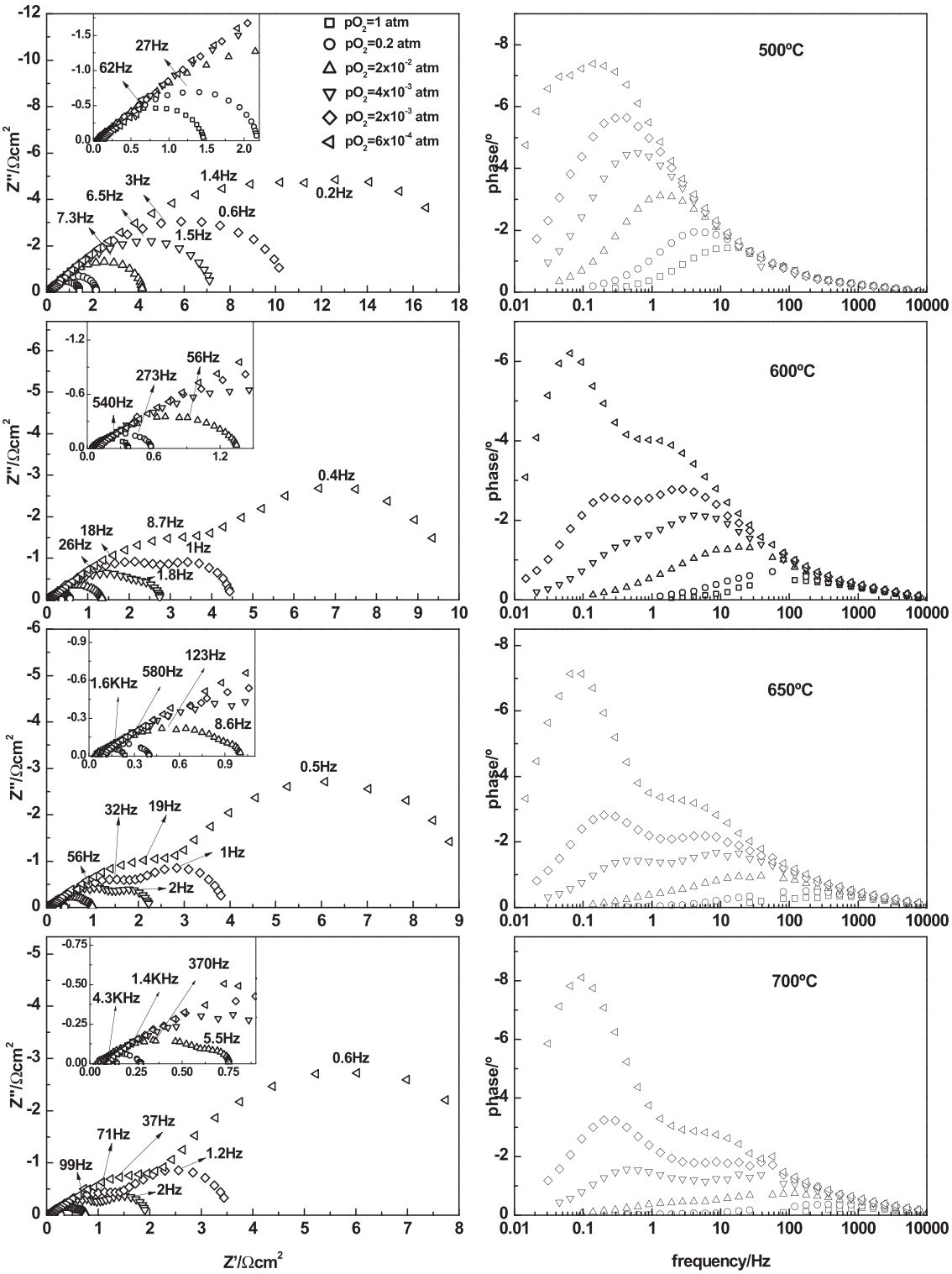

Fig. 6. Nyquist (left) and Bode (right) plots of the EIS spectra obtained for symmetric cells with NSFC as electrode, at temperatures and atmospheres with different pO_2.

vacancy mechanism involving the O(4) and O(2) crystal sites through O(4)-O(4) and O(4)-O(2) jumps along the (Fe,Co)(1)O_6 octahedra edge [13], while O(1) and O(3) crystal sites remain fully occupied. Hence, even if only the O(2) and O(4) crystal sites are considered to participate in the oxygen ion diffusion, the fraction of unoccupied oxygen crystal sites according to NPD and thermogravimetric data [13] result < 1/4. Thus, σ_{ion} should increase as pO_2 decreases, which is the opposite of the experimental data behavior. This inconsistency was also observed for $Sr_3FeMO_{6+\delta}$ (M = Fe, Co, Ni) [17] electrodes, where three instead of two impedance arcs were observed for these $n = 2$ RP phases with a perovskite block with two perovskite layers. Then, although the election of the circuit element for the intermediate frequency contribution is not evident, henceforward, the impedance data was analyzed using a Warburg element.

The fitting parameters and goodness (χ^2) of the fits of EIS spectra of PSFC cell, at 700 °C at all the measured pO_2 values, are summarized in

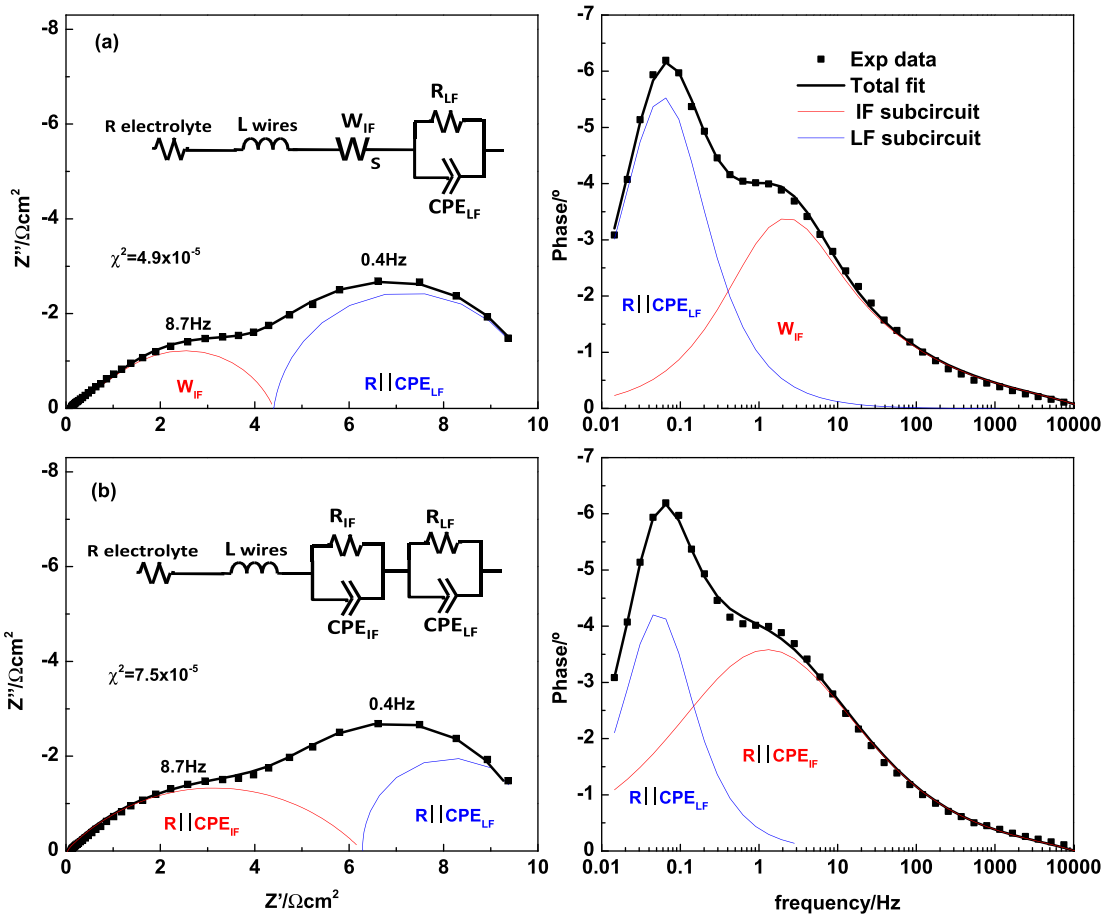

Fig. 7. EIS spectrum (Nyquist left Bode right) of NSFC cell at 600 °C at $pO_2 = 6 \times 10^{-4}$ atm fitted using: (a) a Whf- R||CPE_{LF} circuit; (b) a R||CPE_{IF}-R||CPE_{LF} circuit.

Table 2. All fits made with the same circuit on the spectra shown in Fig. 6 yielded similar quality with exponent values of $0.32 < p_{IF} < 0.5$ (W_{IF}) and $0.75 < p_{LF} < 1$ (R||CPE_{LF}).

Fig. 8a shows the log R_{IF} vs. log pO_2 data for the three electrodes at various temperatures. The exponent m obtained from the slope displayed at 500 °C was close to $m \sim -0.25$. This value is expected when the limiting step is the charge transfer process at the electrode surface, including reduction of the adsorbed atomic oxygen and oxide ion incorporation into the cathode lattice ($O_{ads} + 2e^- + V_{\ddot{O}} \leftrightarrow O_O^x$). However, the capacitance for this impedance arc is in the range of 3.4×10^{-2} to 2.7×10^{-1} F cm^{-2}, which is in between those expected for the charge transfer process at the electrode surface (10^{-3}–10^{-5} Fcm^{-2}) and oxygen diffusion in the bulk (0.1–1 Fcm^{-2}) [25,26], suggesting a mixed contribution for the intermediate impedance arc. As the temperature increases from 500 °C to 700 °C, the parameter m slightly shifts to more negative values $m \sim -0.35$ suggesting that the dissociation of molecular to atomic oxygen at the surface of the electrode ($O_{2,ads} \leftrightarrow 2O_{ads}$) increases its relevance as limiting process.

This trend for the intermediate frequency contribution was also reported for the cobaltites $Ba_{0.5}Sr_{0.5}Co_{0.8}Fe_{0.2}O_{3-\delta}$ [33] and $La_{0.5}Ba_{0.5}CoO_{3-\delta}$ [34] and for the $n = 2$ R-P phases $Sr_3Fe_2O_{7-\delta}$ and $Sr_3FeCoO_{7-\delta}$ [17]. However, a R||CPE element was used in the case of the cobaltites and a Warburg element for the $n = 2$ R-P phases. We believe that a more detailed work is required to clarify the necessity of a diffusive process to reproduce the impedance spectra at various pO_2 in these R-P phases. In Fig. 8b, the linear dependence of R_{IF} with T^{-1} indicates a thermally activated process in the whole temperature range with activation energies increasing as the pO_2 does. For example, for PSCF, the activation energy increases from 0.52 eV at $pO_2 = 6 \times 10^{-4}$ atm to 0.85 eV at $pO_2 = 1$ atm. The lowest R_{IF} at a given pO_2 were obtained for the PSFC electrodes.

The variations of the polarization resistance R_{LF} with the oxygen partial pressure at various temperatures for the LSCF, NSFC and PSFC

Table 2
Parameters from EIS fitting with W_{IF}-RCPE_{LF} circuit of PSFC cell at 700 °C. B and p are frequency independent parameters from a Warburg or an R||CPE element whereas C and f are the capacitance and the relaxation frequency of each semi-circle.

pO_2/atm	W_{IF}					R||CPE_{LF}					$\chi^2 \times 10^{-6}$
	R_{IF}/Ωcm^2	B_{IF}	p_{IF}	C_{IF}/Fcm^{-2}	ν_{IF}/Hz	R_{LF}/Ωcm^2	B_{LF}	p_{LF}	C_{LF}/Fcm^{-2}	ν_{LF}/Hz	
1	0.051	0.001	0.394	0.277	4915						9.8
0.2	0.105	0.002	0.354	0.232	1668						6.4
2×10^{-2}	0.226	0.007	0.347	0.240	340	0.082	0.481	0.883	1.844	4.3	1.4
4×10^{-3}	0.374	0.018	0.350	0.223	143	0.492	0.234	0.839	0.996	1.6	1.9
2×10^{-3}	0.500	0.031	0.344	0.222	80	1.158	0.177	0.853	0.842	1.0	1.6
6×10^{-4}	0.810	0.074	0.323	0.211	34	3.624	0.129	0.879	0.690	0.5	7.1

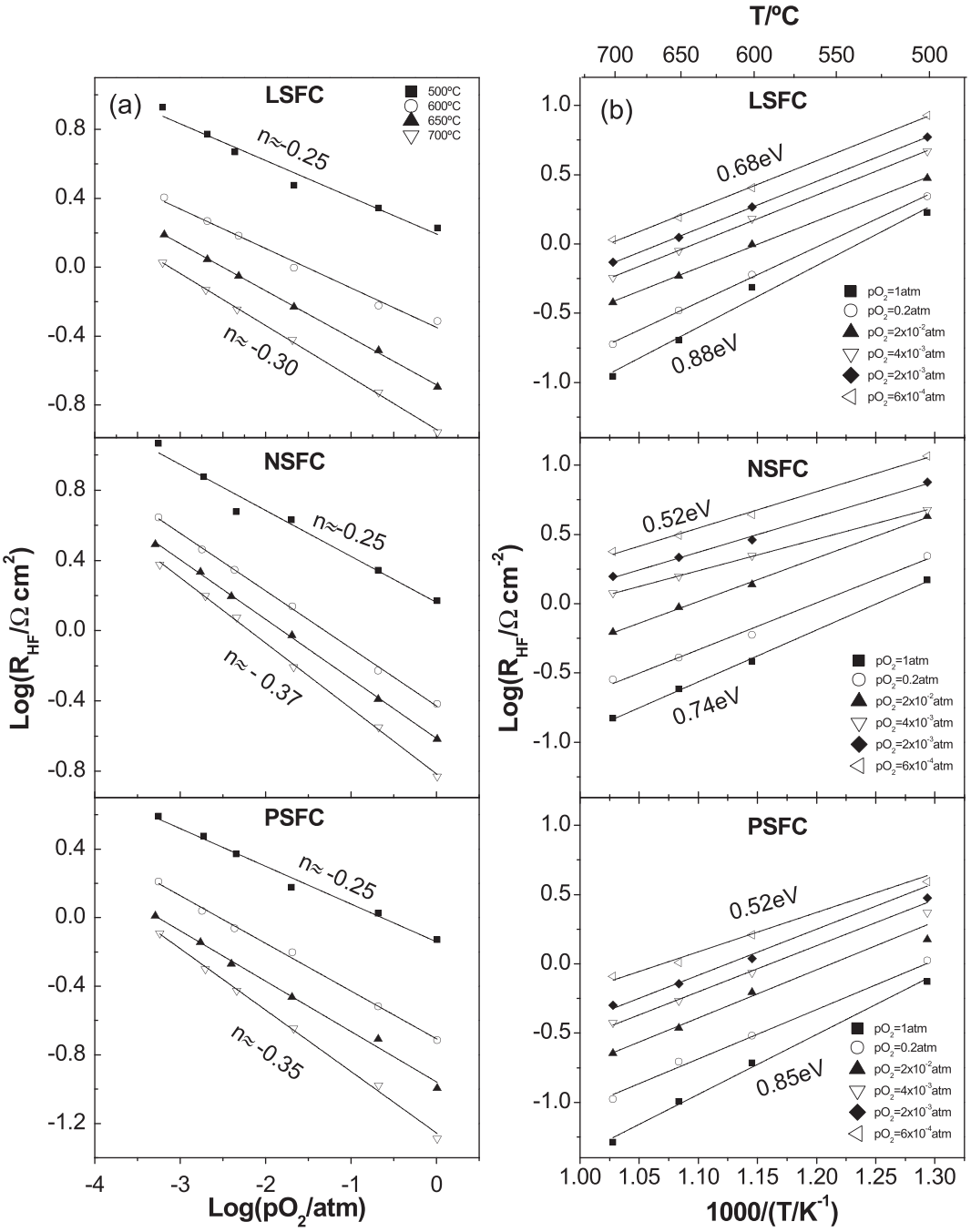

Fig. 8. Intermediate frequency contribution to the polarization resistance R_{IF}, fitted with a W_{IF} element, as a function of: (a) pO_2 at different temperatures; (b) temperature at different pO_2.

electrodes are shown in Fig. 9. The insets show that at $T \geq 600$ °C, R_{LF} exhibits a weak or null variation with temperature for a given pO_2. Nevertheless, lowering temperature down to 500 °C there is an increase of R_{LF} for the three cells suggesting changes in the limiting step involved in the low frequency semi-circle. This behavior is also observed in the slope of the log (R_{LF}) vs log (pO_2/atm) data at constant temperature, displayed in Fig. 9, which is related to the exponent m of Eq. (1). At $T \geq 600$ °C the exponent m is close to -1 for the three cells. At 500 °C, the slope of the linear regression is approximately $m = -0.5$ for NSCF and $m = -0.67$ and -0.68 for LSFC and PSFC, respectively. Another characteristic of the low frequency contribution is the range of the capacitance calculated from the parameters obtained upon fitting the $R||CPE_{LF}$ contribution. The capacitance values for the three electrodes are in the range $1 \times 10^{-1} \leq C_{LF} \leq 5\,F/cm^2$, while the characteristic frequencies vary in the range $1 \times 10^{-1}\,Hz \leq \nu_{LF} \leq 8\,Hz$. The slight variation of R_{LF} with temperature at $T \geq 600$ °C, the value $m \sim -1$ for the slope of the log (R_{LF}) vs log (pO_2/atm) data, the magnitudes of the capacitance and apex frequencies of this contribution suggest this process is associated to the oxygen gas diffusion through the electrode pores, which typically presents capacitance values between 0.1 and 10 Fcm^{-2} [25]. This limiting stage of the ORR, previously observed in other mixed conductor oxides electrodes by impedance spectroscopy, becomes important only at high temperature and does not exhibit thermal activation [33]. However, the parameter m values between -0.5 and -1, at $T = 500$ °C suggests the LF contribution at this temperature might be the consequence of the

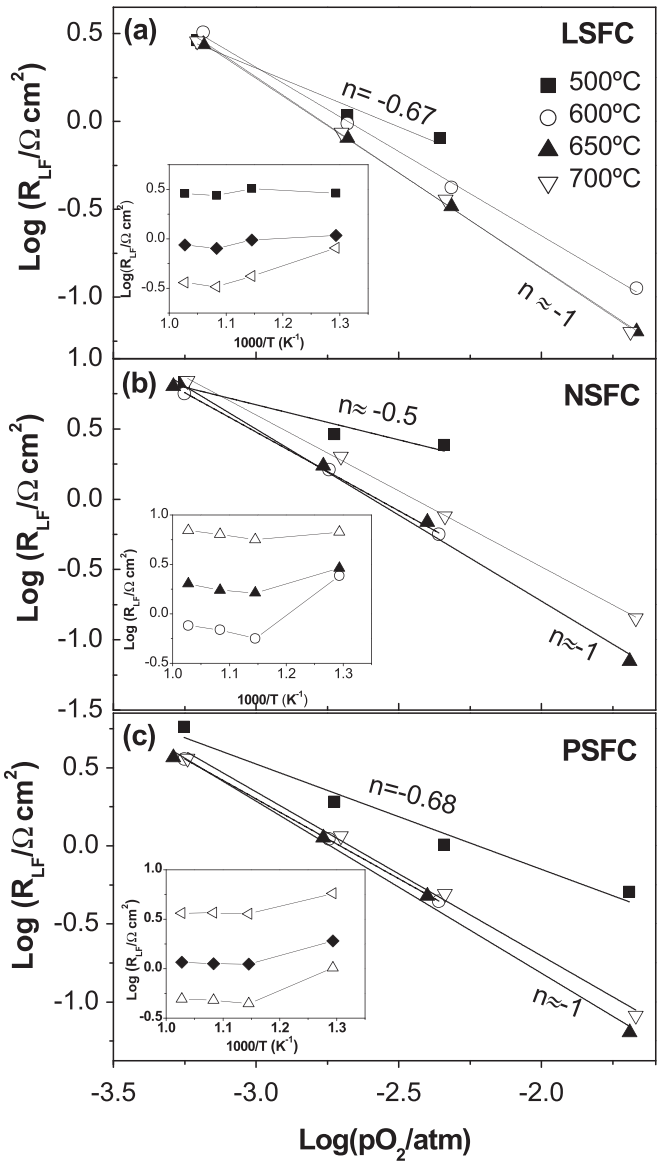

Fig. 9. Low frequency contribution to the polarization resistance R_{LF} as a function of pO_2 at different temperatures; dependence on temperature at different pO_2 in the inset.

convolution of two processes, molecular dissociative adsorption [25,27] and oxygen gas diffusion through the electrode pores.

4. Conclusions

The polarization resistance of electrodes prepared with the $n = 3$ RP phases LSFC, NSFC and PSFC were studied by EIS on symmetrical cells, as a function of thickness, temperature and pO_2. *Rp* shows no variation for NSCF and PSCF electrodes when the thickness was varied from 6 to 19 μm, while for LSFC it decreases as the thickness of the electrode increases up to 20 μm. This behavior was assigned to variations in the characteristic length of the materials. Two impedance arcs, one at intermediate frequencies and another one at lower frequencies, visible mainly at low pO_2, were observed in the EIS spectra of all three analyzed electrodes. For the low frequency contribution we found that oxygen diffusion through the porous of the electrode becomes relevant above 600 °C. The intermediate frequency contribution was associated to the colimitation of the oxygen adsorption plus charge transfer at the electrode surface ($m \sim -0.25$) with an oxide ion diffusive process. When temperature increases from 500 to 700 °C, the molecular oxygen dissociation step at the electrode surface becomes more significant as the parameter m shift towards -0.5. The lowest overpotentials for oxygen reduction of the series LSFC, NSFC and PSFC were obtained for the $PrSr_3Fe_{1.5}Co_{1.5}O_{10-\delta}$ electrode. More research is needed to address the potential of these $n = 3$ RP phases as oxide mixed conductor.

Acknowledgment

This work was supported by Consejo Nacional de Investigaciones Científicas y Técnicas (CONICET) and Agencia Nacional de Promoción Científica y Técnica (ANPCyT), Argentina, through PIP 112 2013 0100151 CO and PICT 2013-1032 and 2016-1921, respectively.

Appendix A. Supplementary data

Supplementary data to this article can be found online at https://doi.org/10.1016/j.ssi.2018.08.020.

References

[1] S.N. Ruddlesden, P. Popper, The compound $Sr_3Ti_2O_7$ and its structure, Acta Crystallogr. 11 (1958) 54–55, https://doi.org/10.1107/S0365110X58000128.
[2] S. Skinner, Oxygen diffusion and surface exchange in $La_{2-x}Sr_xNiO_{4+\delta}$, Solid State Ionics 135 (2000) 709–712, https://doi.org/10.1016/S0167-2738(00)00388-X.
[3] J. Bassat, Anisotropic ionic transport properties in $La_2NiO_{4+\delta}$ single crystals, Solid State Ionics 167 (2004) 341–347, https://doi.org/10.1016/j.ssi.2003.12.012.
[4] E. Boehm, J. Bassat, P. Dordor, F. Mauvy, J. Grenier, P. Stevens, Oxygen diffusion and transport properties in non-stoichiometric $Ln_{2-x}NiO_{4+\delta}$ oxides, Solid State Ionics 176 (2005) 2717–2725, https://doi.org/10.1016/j.ssi.2005.06.033.
[5] L. Minervini, R.W. Grimes, J.A. Kilner, K.E. Sickafus, Oxygen migration in $La_2NiO_{4+\delta}$, J. Mater. Chem. 10 (2000) 2349–2354, https://doi.org/10.1039/b004212i.
[6] T. Armstrong, F. Prado, A. Manthiram, Synthesis, crystal chemistry, and oxygen permeation properties of $LaSr_3Fe_{3-x}Co_xO_{10}$ ($0 \le x \le 1.5$), Solid State Ionics 140 (2001) 89–96, https://doi.org/10.1016/S0167-2738(01)00696-8.
[7] F. Prado, T. Armstrong, A. Caneiro, A. Manthiram, Structural stability and oxygen permeation properties of $Sr_{3-x}La_xFe_{2-y}Co_yO_{7-\delta}$ ($0 \le x \le 0.3$ and $0 \le y \le 1.0$), J. Electrochem. Soc. 148 (2001) J7, https://doi.org/10.1149/1.1354605.
[8] K.T. Lee, A. Manthiram, $LaSr_3Fe_{3-y}Co_yO_{10-\delta}$ ($0 \le y \le 1.5$) intergrowth oxide cathodes for intermediate temperature solid oxide fuel cells, Chem. Mater. 18 (2006) 1621–1626 https://pubs.acs.org/doi/abs/10.1021/cm052645%2B?src=recsys.
[9] S. Chaianansutcharit, Y.W. Ju, S. Ida, T. Ishihara, Ni doped $PrSr_3Fe_3O_{10-\delta}$ Ruddlesden-Popper oxide for active oxygen reduction cathode for solid oxide fuel cell, Electrochim. Acta 222 (2016) 1853–1860, https://doi.org/10.1016/j.electacta.2016.11.178.
[10] S. Chaianansutcharit, K. Hosoi, J. Hyodo, Y.-W. Ju, T. Ishihara, Ruddlesden Popper oxides of $LnSr_3Fe_3O_{10-\delta}$ (Ln = La, Pr, Nd, Sm, Eu, and Gd) as active cathodes for low temperature solid oxide fuel cells, J. Mater. Chem. A 3 (2015) 12357–12366, https://doi.org/10.1039/C5TA01273B.
[11] L. Mogni, F. Prado, A. Caneiro, Defect structure and electrical conductivity of the Ruddlesden – Popper phases $Sr_3FeMO_{6+\delta}$ (M = Co, Ni), Chem. Mater. 18 (2006) 4163–4170, https://doi.org/10.1021/cm0604007.
[12] F. Prado, L. Mogni, G. Cuello, A. Caneiro, Neutron powder diffraction study at high temperature of the Ruddlesden–Popper phase $Sr_3Fe_2O_{6+\delta}$, Solid State Ionics 178 (2007) 77–82, https://doi.org/10.1016/j.ssi.2006.11.014.
[13] F. Prado, A. Abate, J.V.V. Castillo, A. Caneiro, G. Cuello, High temperature crystal chemistry of the n = 3 Ruddlesden-Popper phase $LaSr_3Fe_{1.5}Co_{1.5}O_{10-\delta}$, Solid State Ionics 270 (2015) 54–60, https://doi.org/10.1016/j.ssi.2014.12.007.
[14] I. Kagomiya, K. Jimbo, K. Kakimoto, Distribution change of oxygen vacancies in layered perovskite type$(Sr, La)_{n+1}FenO_{3n+1}$ (n = 3), J. Solid State Chem. 207 (2013) 184–189, https://doi.org/10.1016/j.jssc.2013.08.030.
[15] Y.N. Kim, A. Manthiram, Electrochemical properties of Ln $(Sr,Ca)_3(Fe,Co)_3O_{10}$ + $Gd_{0.2}Ce_{0.8}O_{1.9}$ composite cathodes for solid oxide fuel cells, J. Electrochem. Soc. 158 (2011) B1206, , https://doi.org/10.1149/1.3621718.
[16] K.P. Padmasree, K.Y. Lai, W. Kaveevivitchai, A. Manthiram, Effect of Ca substitution on the electrochemical properties of the Ruddlesden-Popper oxides $Sr_{3.2-x}Ca_xLn_{0.8}Fe_{1.5}Co_{1.5}O_{10-\delta}$, J. Power Sources 374 (2018) 249–256, https://doi.org/10.1016/j.jpowsour.2017.11.047.
[17] L. Mogni, N. Grunbaum, F. Prado, A. Caneiro, Oxygen reduction reaction on Ruddlesden–Popper phases studied by impedance spectroscopy, J. Electrochem. Soc. 158 (2011) B202, https://doi.org/10.1149/1.3511770.
[18] J. Rodríguez-Carvajal, Recent advances in magnetic structure determination by neutron powder diffraction, Phys. B Condens. Matter 192 (1993) 55–69, https://doi.org/10.1016/0921-4526(93)90108-I.
[19] S.J.A. Figueroa, J.C. Mauricio, J. Murari, D.B. Beniz, J.R. Piton, H.H. Slepicka, M.F. De Sousa, A.M. Espíndola, A.P.S. Levinsky, Upgrades to the XAFS2 beamline control system and to the endstation at the LNLS, J. Phys. Conf. Ser, IOP Publishing,

2016, p. 012022, , https://doi.org/10.1088/1742-6596/712/1/012022.
[20] B. Ravel, M. Newville, ATHENA, ARTEMIS, HEPHAESTUS: data analysis for X-ray absorption spectroscopy using IFEFFIT, J. Synchrotron Radiat. 12 (2005) 537–541, https://doi.org/10.1107/S0909049505012719.
[21] A. Caneiro, M. Bonnat, J. Fouletier, Measurement and regulation of oxygen content in selected gases using solid electrolyte cells. IV. Accurate preparation of CO_2-CO and H_2O-H_2 mixtures, J. Appl. Electrochem. 11 (1981) 83–90, https://doi.org/10.1007/BF00615326.
[22] I.D.J. ZView™ version 2.0b copyright 1990–2005, Scribner Associates, A Software Program for IES Measurements and Analysis, http://www.scribner.com/zview-for-windows.html, (2007) , Accessed date: 23 August 2011.
[23] R.D. Shannon, Revised effective ionic radii and systematic studies of interatomic distances in halides and chalcogenides, Acta Crystallogr. Sect. A. 32 (1976) 751–767, https://doi.org/10.1107/S0567739476001551.
[24] T.W. Capehart, R.K. Mishra, J.F. Herbst, Direct determination of praseodymium valence in $Pr_2(Co_xFe_{1-x})_{14}B$, J. Appl. Phys. 72 (1992) 676–679, https://doi.org/10.1063/1.351851.
[25] S.B. Adler, Factors governing oxygen reduction in solid oxide fuel cell cathodes, Chem. Rev. 104 (2004) 4791–4843, https://doi.org/10.1021/cr020724o.
[26] S.B. Adler, J.A. Lane, B.C.H. Steele, Electrode kinetics of porous mixed-conducting oxygen electrodes, J. Electrochem. Soc. 143 (1996) 3554, https://doi.org/10.1149/1.1837252.
[27] Y. Takeda, R. Kanno, M. Noda, Y. Tomida, Y. O, Cathodic polarization phenomena of perovskite oxide electrodes with stabilized zirconia, J. Electrochem. Soc. 134 (1987) 2656, https://doi.org/10.1149/1.2100267.
[28] A. Ringuedé, J. Fouletier, Oxygen reaction on strontium-doped lanthanum cobaltite dense electrodes at intermediate temperatures, Solid State Ionics 139 (2001) 167–177, https://doi.org/10.1016/S0167-2738(01)00692-0.
[29] C. Deportes, M. Duclot, P. Fabry, Electrochimie des solides, Presses Universitaires de Grenoble, 1994, https://www.grenoble-sciences.fr/ouvrage/electrochimie-des-solides-isbn-9782868834478 (accessed June 14, 2018).
[30] C.-Y. Yoo, D.S. Yun, S.-Y. Park, J. Park, J.H. Joo, H. Park, M. Kwak, J.H. Yu, Investigation of electrochemical properties of model lanthanum strontium cobalt ferrite-based cathodes for proton ceramic fuel cells, Electrocatalysis 7 (2016) 280–286, https://doi.org/10.1007/s12678-016-0306-1.
[31] J.R. MacDonald, Note on the parameterization of the constant-phase admittance element, Solid State Ionics 13 (1984) 147–149, https://doi.org/10.1016/0167-2738(84)90049-3.
[32] J.B. Goodenough, Review lecture: fast ionic conduction in solids, Proc. R. Soc. A Math. Phys. Eng. Sci. 393 (1984) 215–234, https://doi.org/10.1098/rspa.1984.0055.
[33] C. Setevich, F. Prado, A. Caneiro, Electrochemical response of several cathode configurations prepared with $Ba_{0.5}Sr_{0.5}Co_{0.8}Fe_{0.2}O_{3-\delta}$ and $Ce_{0.9}Gd_{0.1}O_{1.95}$ for IT-SOFC, J. Solid State Electrochem. 20 (2016) 1633–1643, https://doi.org/10.1007/s10008-016-3172-0.
[34] S. Pang, X. Jiang, X. Li, Q. Wang, Z. Su, A comparative study of electrochemical performance of $La_{0.5}Ba_{0.5}CoO_{3-\delta}$ and $La_{0.5}Ba_{0.5}CoO_{3-\delta}$–$Gd_{0.1}Ce0_{.9}O_{1.95}$ cathodes, Int. J. Hydrog. Energy 37 (2012) 2157–2165, https://doi.org/10.1016/J.IJHYDENE.2011.09.156.